Morris, J.D., Villinger, H.W., and Klaus, A. (Eds.)
Proceedings of the Ocean Drilling Program, Scientific Results Volume 205

5. Data Report: Chemical and Isotopic Compositions of Pore Fluids and Sediments from across the Middle America Trench, offshore Costa Rica[1]

Miriam Kastner,[2] Evan Solomon,[2] Wei Wei,[2] Lui-H. Chan,[3] and Ola M. Saether[4]

ABSTRACT

Pore fluid and sediment chemical and isotopic data were obtained for samples from Ocean Drilling Program (ODP) Leg 205 Sites 1253, 1254, and 1255 in the Costa Rica subduction zone. The chemical and isotopic data reported here were generated in our shore-based laboratories to complement shipboard inorganic geochemical data. Li isotopic analyses were carried out by L.-H. Chan at Louisiana State University (USA). The data reported herein include fluoride, bromide, rubidium, cesium, and barium concentrations; Li and Sr isotopic compositions in pore fluids; and Rb, Cs, and Ba concentrations in representative bulk sediments. The data also include new pore fluid fluoride and bromide concentrations from corresponding ODP Leg 170 Sites 1039, 1040, and 1043. O.M. Saether's Site 1039 and 1040 fluoride concentration data are shown for comparison. Basal sediment fluoride concentrations and Li and Sr isotope ratios at both Sites 1253 and 1039 show reversals that approach modern seawater values. Br/Cl ratios are, however, conservative throughout the sediment section at Sites 1039 and 1253. The observed sharp F and Br concentration maxima, Rb and K concentration minima, the most radiogenic $^{87}Sr/^{86}Sr$ ratios, and highest δ^7Li values along the décollement and fracture zone (Sites 1040, 1043, 1254, and 1255) strengthen the evidence obtained during Leg 170 that a deeply sourced fluid, originating from fluid-rock reactions at ~150°C and correspond-

[1] Kastner, M., Solomon, E., Wei, W., Chan, L.-H., and Saether, O.M., 2006. Data report: Chemical and isotopic compositions of pore fluids and sediments from across the Middle America Trench, offshore Costa Rica. *In* Morris, J.D., Villinger, H.W., and Klaus, A. (Eds.), *Proc. ODP, Sci. Results,* 205, 1–21 [Online]. Available from World Wide Web: <http://www-odp.tamu.edu/publications/205_SR/VOLUME/CHAPTERS/208.PDF>. [Cited YYYY-MM-DD]
[2] Scripps Institution of Oceanography, University of California San Diego, La Jolla CA 92093-0212, USA. Correspondence author: **mkastner@ucsd.edu**
[3] Department of Geology and Geophysics, Louisiana State University, Baton Rouge LA 70803-4101, USA.
[4] Geological Survey of Norway, Postboks 3006 Lade, N-7002 Trondheim, Norway.

Initial receipt: 11 March 2005
Acceptance: 7 June 2006
Web publication: 28 September 2006
Ms 205SR-208

ing to between 10 and 15 km depth, is transporting solutes to the ocean.

An additional interesting observation is the positive relationship between F and Ca concentrations, both at the oceanic reference sites (1039 and 1253) and particularly in the décollement and fracture zone at Sites 1040 and 1254. The origin of this relationship is being investigated. Fluoride, an important metal-complexing agent, is highly enriched in the deep-sourced fluid identified at Sites 1040 and 1254. Complexation with F may therefore help to explain some of the observed trace metal concentrations in arc volcanic rocks.

INTRODUCTION

Ocean Drilling Program (ODP) Leg 205 returned to the Middle America Trench to install long-term observatories in order to investigate the active fluid flow across the Costa Rica margin and its implications for the seismogenic zone and subduction factory. This was achieved by installing circulation obviation retrofit kit (CORK)-IIs at two sites across the Middle America Trench offshore Costa Rica, previously drilled during ODP Leg 170 (Kimura, Silver, Blum, et al., 1997; Morris, Villinger, Klaus, et al., 2003) that were instrumented for long-term monitoring of pressure and temperature and for collecting time series of fluid and gas samples for subsequent chemical analysis (Jannasch et al., 2003). Sediment coring, therefore, focused on the décollement zones at the prism sites (1254 and 1255, corresponding to Leg 170 Sites 1040 and 1043, respectively) and basement drilling at the incoming plate Site 1253 (Leg 170 Site 1039). Because of this, few new pore fluid and sediment samples were obtained during Leg 205. The distinct pore fluid chemical signals across the décollement zones observed during Leg 170 (Kimura, Silver, Blum, et al., 1997) were used to identify the décollement zones at the adjacent sites drilled during Leg 205. At the incoming plate, Site 1253, pore fluids and sediment samples were obtained only from the basal sediment section. Diagenesis was observed in the overlying sediments and between sills, and correspondingly, the pore fluids of the most altered sediments were modified as well.

Tracers of interest to geochemists in constraining the extent of smectite-illite reaction in the updip fluid source region and deciphering the bulk composition and temperature of the fluid source region include concentration ratios such as K/Li or K/Rb, F/Cl, and B and Cl isotope ratios. Halogen concentration ratios are presented below; however, because of mass spectrometer instrument problems, Cl and B isotope ratio data sets are incomplete. Preliminary results of the pore fluid Cl isotopic compositions indicate that at Sites 1040 and 1254, the $\delta^{37}Cl$ values in décollement and fracture zone pore fluids are more negative than the values in prism and underthrust sediments. Tracers of interest to geochemists for tracking element recycling in volcanic arcs by subduction (e.g., Rb, Cs, Sr, and Ba concentrations and Sr and Li isotope ratios) were analyzed in the fluids and are reported in Tables T1 and T2. When flow rates are established using data generated by ongoing monitoring of deep-sourced fluids, flux rates for elements leaving the subducting plate in fluid advected from deeper sources will be calculated. Such data will be useful for evaluating the impact of shallow slab dewatering on ocean chemistry and on composition of the residual slab subducted deeper (ultimately to depths of magma generation).

T1. Chemical and Li isotope compositions, p. 20.

T2. Ba, Rb, and Cs concentrations, p. 21.

The tracers chosen for pore fluid analysis from the Costa Rica subduction zone have two important characteristics:

1. Some tracers identify fluid-rock reactions (i.e., Li, B, Sr, and Ba), or specifically fluid-hydrous mineral reactions and mobility in the subduction zone (F, Cl, and Br).
2. Other tracers provide information on the approximate temperature of reaction (Li, K, Rb, and Cs) or on the sources and mixing of fluids involved in different fluid-rock reactions (Li, Sr, Cl, and O isotope ratios). Some of these are particularly important because they also are not involved in key retrograde reactions during migration (i.e., Cl, Br, and, possibly, F), thus, they maintain their identity even when mixed with diagenetic fluids formed in situ along the flow lines.

Because the geochemical behavior of halogens (F, Cl, and Br) is dominated by strong partitioning into the fluid phase, they are excellent tracers of fluids during subduction. Elemental and isotopic halogen systematics can thus supply critical information not available from other measurements about sources of fluids, flow paths, and reaction conditions. Cl, F, and Br have long been identified as excess volatiles that are thought to have accumulated in seawater, their principal exogenic reservoir, by outgassing of the mantle or from a late accretion of volatile-rich material (Rubey, 1951; Schilling et al., 1978; Jambon, 1994). Despite their abundances and widespread distribution, the geochemical behavior and cycles of F, Cl, and Br are, as yet, not well documented (Jambon, 1994). Rb and Cs, along with K, Ba, and Sr (also La, Th, and U, for which data are not presented) are enriched in arc volcanics worldwide. They are large ion lithophile elements. Rb and Cs concentrations are not routinely measured in pore fluids from ODP legs; however, there have been several recent hydrothermal experiments that investigated their mobility as a function of temperature using representative sediments and seawater (James et al., 2003; W. Wei, pers. comm., 2005). Rb and Cs behave similar to K at low temperatures and are typically partitioned into solids; however, Rb and possibly Cs concentrations increase in the fluid as a result of ion exchange with NH_4 in the sulfate reduction zone. Each of the alkali metals (Li, K, Rb, and Cs) has a characteristic behavior with respect to partitioning into the fluid phase as a function of temperature (W. Wei, pers. comm., 2005). In general, at moderate to high temperatures (>60°C) the alkali metals partition into the fluid phase, with Cs partitioning earlier than Rb.

Primary Results from Site 1039, Supported by Shipboard Data from Site 1253

Strong evidence for vigorous, shallow flow of cool fluids in the oceanic section of the subducting plate at Site 1039 that may affect the updip limit of seismicity was obtained during Leg 170 and is supported by Leg 205 shipboard data. At the locations of the Leg 170 and 205 sites, heat flow is ≤15% of that expected for the plate age, implying significant advection of cool fluids (Langseth and Silver, 1996). Heat flow data taken during recent cruises show that seamounts are sites of fluid discharge and recharge (Fisher et al., 2003b), and modeling suggests that lateral flow rates of 3–30 m/yr in zones within the upper 600 m of high-permeability basement (10^{-10} to 10^{-8} m^2) are required to match the low

heat flow on East Pacific Rise (EPR)-generated crust (Fisher et al., 2003a). Chemical data also suggest vigorous and recent/contemporaneous fluid flow. The active flow system consists of slightly modified modern seawater within the upper oceanic crust (Silver et al., 2000; Kastner et al., 2000). For example, Sr chemical and isotopic values in basal sediments are distinct from those appropriate for seawater of the sediment age or for pore fluid compositions modified by ash weathering, as seen higher in the sediment column (Silver et al., 2000). Simple modeling suggests that the gradients, also observed for Li, Ca, and SO_4, would diffuse away in ~15 k.y., unless supported.

Primary Results from Prism Sites 1040 and 1043, Supported by Shipboard Data from Sites 1254 and 1255

At the décollement sites (1040, 1043, 1254, and 1255), pore fluid samples from the plate boundary and fault zone above it show strong, narrow anomalies in the abundances of thermogenic hydrocarbons through C_6 and other tracers (e.g., Ca, K, and Li). Taken together, the compositional anomalies indicate vigorous advection within the décollement and fault zones that transports species generated at temperatures of ~150°C (i.e., at or near temperatures thought to occur at the updip limit of the seismogenic zone). The persistence of local compositional anomalies suggests transient flow.

MATERIALS AND METHODS

All pore fluids analyzed were obtained by routine shipboard squeezing of whole-round sediment samples almost immediately after retrieval. The sediments were squeezed in titanium squeezers at ambient temperature and pressures of 2000–3000 psi (140–210 kg/cm²). Samples were analyzed on board for a range of constituents (Morris, Villinger, Klaus, et al., 2003) and were supplemented by shore-based analyses summarized in Tables **T1** and **T2.** F and Br (Figs. **F1, F2, F3**) were analyzed by ion chromatography with a precision of 3%–5% after diluting the pore fluids (typical dilution ratio = 10). Saether's F concentration data were obtained with ion selective electrodes with a detection limit of 0.1 ppm. The error reported is 0.7% and the standard deviation is 3.6%. Rb, Cs, and Ba concentrations in both pore fluids and sediments (Figs. **F4, F5, F6, F7**) were analyzed by inductively coupled plasma–mass spectroscopy (ICP-MS; ThermoQuest/Finnigan Element 2). The pore fluid samples and standards were diluted with 0.4-N HNO_3 and spiked with a 1.0-ppb In internal standard. Twenty pore fluid samples and a 0.5- and 2.0-ppb standard were analyzed in each batch of analyses. A 1.0-ppb drift standard was analyzed after every four samples. Instrumental drift was corrected online by normalization of the intensity of the analyte with that of the ^{115}In standard. A second drift correction was applied offline using repeated analyses of the 1.0-ppb Ba, Rb, and Cs drift standard made by dilution of the primary stock solution. The accuracy and precision of multiple analyses were determined by repeated analyses of the 1.0- ppb drift standard, as well as the 0.5- and 2.0-ppb standards. The average accuracies for Ba, Rb, and Cs were <1%, <1%, and <2%, respectively, and the average precisions of the Ba, Rb, and Cs analyses were <0.65%, 0.5%, and <2%, respectively. An addi-

F1. F and F/Cl, p. 9.

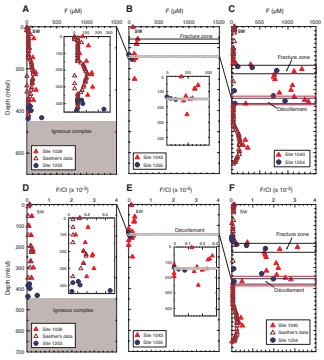

F2. Br and Br/Cl, p. 10.

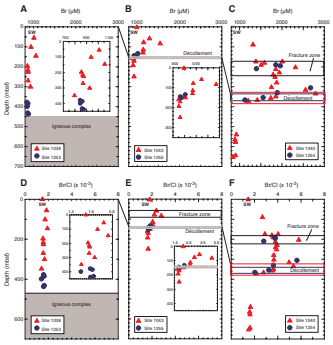

F3. F and Ca, p. 11.

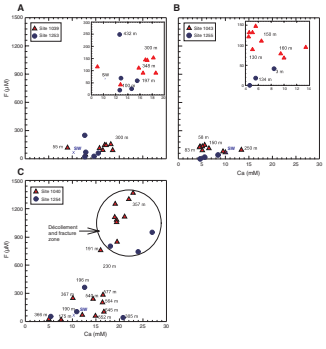

F4. Rb and Cs, p. 12.

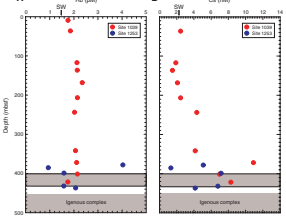

tional 65 pore fluid samples were analyzed for Ba concentrations by standard addition on a Perkin Elmer Optima 3000 ICP–optical emission spectrometer (OES) (Figs. F6, F7, F8). The average accuracy and precision of the ICP-OES analyses determined by multiple analyses of drift and calibration standards were <4% and <7%, respectively. The results of ICP-MS and ICP-OES determinations agree well (Figs. F6, F7, F8).

The sediment samples were digested by adding 4-N HNO_3 to dissolve the carbonate, 30% hydrogen peroxide to oxidize the organic matter, a 2:1 mixture of concentrated hydrofluoric (HF) and nitric (HNO_3) acids to digest the sample, and then two portions of concentrated nitric acid. The digested samples were diluted with a 2% Optima nitric acid solution. All solutions were spiked with a 1.0-ppb In internal standard. The method of analysis by ICP-MS was identical to that performed on the pore fluid samples outlined above. The precision and accuracy of the sediment digestion protocol were determined by repeated digestions of reference U.S. Geological Survey (USGS) certified rock standards MAG-1 (marine mud) and SCO-1 (Cody shale). The average percent accuracies of multiple determinations of these standards for Ba, Rb, and Cs were <1%, 1.9%, and 3.5%, respectively, and the average percent precisions for Ba, Rb, and Cs were <1%, ~1%, and 1.3%, respectively. The Ba concentration data are from **Solomon et al.** (this volume). Some shipboard X-ray fluorescence (XRF) data analyzed during Leg 170 are included in Figures F6 and F7. The samples were measured on an ARL 8420 XRF with reported percent accuracy and precision of 2%–3% (Kimura, Silver, Blum, et al., 1997).

Isotopic compositions of pore fluids and bulk solids were determined by thermal ionization mass spectrometry (TIMS) according to the procedures previously described in Paytan et al. (1993) for Sr isotope ratios and You and Chan (1996) and Chan and Kastner (2000) for Li isotope ratios. Sr and Li concentrations were determined on board by ICP-atomic emission spectroscopy (Morris, Villinger, Klaus, et al., 2003). Sr isotope ratios (Fig. F9) were determined at Scripps Institution of Oceanography (SIO; California, USA) and Li isotope ratios (Fig. F10) were determined at Louisiana State University. The 2σ errors in Sr isotope ratio run uncertainties are smaller than the external precision of ±0.000024. The modern seawater value (NASS-2) measured at SIO is 0.709175 ± 24. All ratios are normalized to $^{86}Sr/^{88}Sr = 0.1194$. The $^{87}Sr/^{86}Sr$ ratio of the National Bureau of Standards (NBS) standard measured at the SIO laboratory is 0.710260 ± 24. Li isotope ratios of pore fluids were determined using Li_3PO_4 as an ion source material. The precision of both methods is ~1%. Li isotope ratios are reported as δ^7Li relative to National Institute of Standards and Testing (NIST) standard LSVEC. The $^7Li/^6Li$ of the standard determined by the phosphate method during the course of the study was 12.0844 ± 0.0088 (2σ).

PRIMARY RESULTS

In addition to the Leg 205 pore fluids analyzed for F, Br, Ba, Rb, and Cs concentrations and $^{87}Sr/^{86}Sr$ and δ^7Li values and bulk sediments analyzed for Ba, Rb, and Cs concentrations, Leg 170 pore fluids were also analyzed for F and Br concentrations.

Fluoride concentrations and $^{87}Sr/^{86}Sr$ and $^7Li/^6Li$ ratios in the basal sections of Sites 1039 and 1253 (Figs. F1, F3, F9, F10, F11) show the same reversals in concentrations and isotope ratios that approach mod-

F5. K and Rb, p. 13.

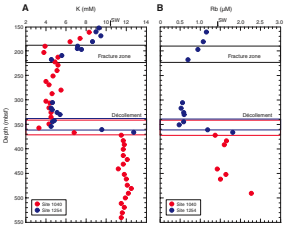

F6. Rb, Cs, and Ba, Sites 1039 and 1253, p. 14.

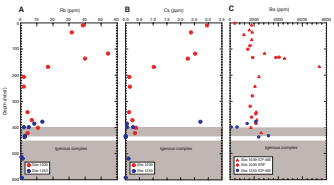

F7. Rb, Cs, and Ba, Sites 1040 and 1254, p. 15.

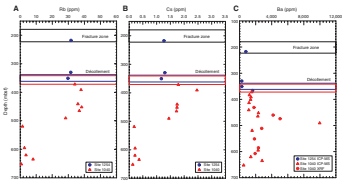

F8. Ba, p. 16.

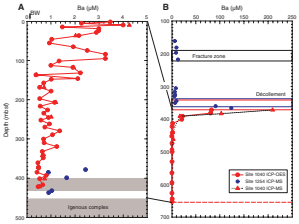

F9. $^{87}Sr/^{86}Sr$ and 1/Sr, p. 17.

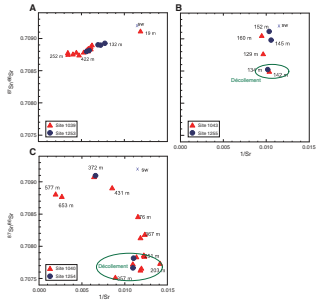

ern seawater values as observed during Leg 170. Site 1253 is ~1.5 km closer to the trench than Site 1039, suggesting that the observed trends are regional. These chemical and isotopic trends are driven by a fluid flow system in the upper igneous complex and/or basement that governs the transport of heat in this section of the downgoing slab. A preliminary model for this fluid flow system was provided by Silver et al. (2000). Similar to Cl concentrations, Br concentrations do not show a reversal in the basal sediments. Because of the high concentration of Br, the Br/Cl ratios at Sites 1039 and 1253 (Fig. **F2**) are conservative throughout the sediment section. The apparent increase in F concentration in the pore fluids of the transition zone between the hemipelagic and pelagic calcareous sections at Sites 1039 and 1253 (Fig. **F1A**) is not seen when the data are normalized to Cl concentrations (Fig. **F1D**).

The most striking observations at the décollement and fracture zones at Sites 1040 and 1254 are

1. The sharp maxima in F and Br concentrations that when normalized to Cl concentrations remain distinct (Figs. **F1C, F1F, F2C, F2F**),
2. The minima in Rb and K concentrations (Fig. **F5**),
3. The less radiogenic Sr isotope ratios at these same horizons (Figs. **F9, F11**), and
4. The lower δ^7Li values (Fig. **F10**).

These data, together with shipboard and Leg 170 geochemical data, constrain the source depth of the fluid transporting solutes to the ocean along the décollement and fracture zones to a source at ~150°C. As discussed in Silver et al. (2000), this temperature corresponds to10–15 km depth. These signals are subdued at Sites 1043 and 1255 because of their proximity to the trench; therefore, they are more dilute.

Additional Important Observations

1. The origin of the positive relationship between F and Ca concentrations both at the oceanic reference Sites 1039 and 1053 and particularly in the décollement and fracture zones observed at Sites 1040 and 1254 (Fig. **F3**) is being investigated. The observation that the deep-sourced fluid is enriched in F, an important metal-complexing agent, may help to explain some of the poorly understood observations of trace metal concentrations in arc volcanic rocks.
2. Organic matter in the prism sediments at Sites 1043 and 1255 and 1040 and 1254 is responsible for the somewhat elevated Br concentrations and Br/Cl ratios (Fig. **F2B, F2C, F2E, F2F**).
3. Barium concentrations are slightly enriched in the hemipelagic and transition zone pore fluids (Site 1039). The organic C content of these sediments is higher than in the calcareous section. The extremely high pore fluid Ba concentrations at Site 1040 below the décollement, in the zone where the sulfate is depleted to zero concentration, is most remarkable (Fig. **F8**), indicating that some of the sediment Ba is being mobilized and returned to the ocean, as discussed by **Solomon et al.** (this volume). The corresponding observed decrease in the sediment Ba concentrations in the hemipelagic section as the plate moves from Sites 1039

F10. δ^7Li, p. 18.

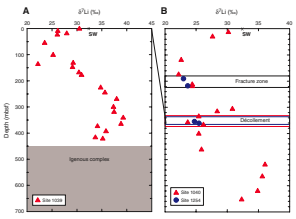

F11. $^{87}Sr/^{86}Sr$, p. 19.

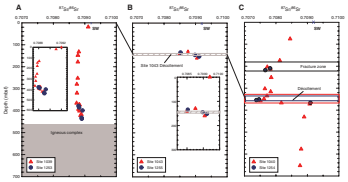

and 1253 to Sites 1040 and 1254 is shown in Figures F6 and F7 and discussed in Solomon et al. (this volume).

4. The concentrations increase with depth at Sites 1039 and 1253, and the behavior of Rb is almost identical to that of K (Figs. F4, F5). This is especially distinct in the décollement and fracture zones at Sites 1040 and 1254, as discussed above. The higher than seawater Rb and K concentrations in the hemipelagic section at Sites 1039 and 1253 are most likely a result of ion exchange reactions between Rb (K) and NH_4. Cesium concentrations are approximately seawater value in the hemipelagic section and increase with depth toward the basal portion of the pelagic sediments. Unlike Ca, Sr, and Li, Cs concentrations increase in the basal section and may reflect communication with a slightly altered fluid system in uppermost basement.

Sediment Rb and Cs concentrations vary with depth at Sites 1039 and 1253 and 1040 and 1254 (Figs. F6, F7), reflecting the relative dilution by biogenic material with distance from the trench. In the hemipelagic sediments Rb and Cs concentrations are >28 ppm and >1 ppm, respectively. At relative plate velocity of 88 km/m.y., Site 1039 was ~440 km from the Middle America Trench at ~5 Ma, thus receiving a mixture of terrigenous and biogenic sediments. In the pelagic carbonates section (with intermittent ash) that was deposited when the plate was closer to the ridgecrest, Rb and Cs concentrations are low (<0 ppm and <0.5 ppm, respectively) and extremely depleted in the basal "baked sediments," most likely because of diagenetically enhanced mobility at moderate to high temperatures (W. Wei, pers. comm., 2005). In the prism section of Sites 1040 and 1254, Rb and Cs concentrations are similar to those in the hemipelagic sediments at the reference Sites 1039 and 1253; however, the average Rb/Cs ratio in the hemipelagic sediments is ~15, and in the prism sediments it is ~25, which may indicate different sources.

ACKNOWLEDGMENTS

We thank the Leg 205 participants for their support and Dr. Michael Mottl for his helpful comments. This research used samples and/or data provided by the Ocean Drilling Program (ODP). ODP is sponsored by the U.S. National Science Foundation (NSF) and participating countries under management of Joint Oceanographic Institutions (JOI), Inc. This research was supported by United States Science Support Program to the Ocean Drilling Program to M.K. and E.S.

REFERENCES

Chan, L.-H., and Kastner, M., 2000. Lithium isotopic compositions of pore fluids and sediments in the Costa Rica subduction zone: implications for fluid processes and sediment contribution to the arc volcanoes. *Earth Planet. Sci. Lett.,* 183:275–290. **doi:10.1016/S0012-821X(00)00275-2**

Fisher, A.T., Davis, E.E., Hutnak, M., Spiess, V., Zühlsdorff, L., Cherkaoui, A., Christiansen, L., Edwards, K.M., Macdonald, R., Villinger, H., Mottl, M.J., Wheat, C.G., and Becker, K., 2003. Hydrothermal recharge and discharge across 50 km guided by seamounts on a young ridge flank. *Nature (London, U. K.),* 421:618–621. **doi:10.1038/nature01352**

Fisher, A.T., Stein, C.A., Harris, R.N., Wang, K., Silver, E.A., Pfender, M., Hutnak, M., Cherkaoui, A., Bodzin, R., and Villinger, H., 2003. Abrupt thermal transition reveals hydrothermal boundary and role of seamounts within the Cocos plate. *Geophys. Res. Lett.,* 30(11). **doi:10.1029/2002GL016766**

Jambon, A., 1994. Earth degassing and large-scale geochemical cycling of volatile elements. *In* Carroll, M.R., and Holloway, J.R. (Eds.), *Volatiles in Magmas*. Rev. Mineral., Mineral. Soc. Am., 30:479–517.

James, R.H., Allen, D.E., and Seyfried, W.E., Jr., 2003. An experimental study of alteration of oceanic crust and terrigenous sediments at moderate temperatures (51 to 350°C): insights as to chemical processes in near-shore ridge-flank hydrothermal systems. *Geochim. Cosmochim. Acta,* 67:681–691. **doi:10.1016/S0016-7037(02)01113-4**

Jannasch, H., Davis, E., Kastner, M., Morris, J., Pettigrew, T., Plant, J.N., Solomon, E., Villinger, H., and Wheat, C.G., 2003. CORK-II: long-term monitoring of fluid chemistry, fluxes, and hydrology in instrumented boreholes at the Costa Rica subduction zone. *In* Morris, J.D., Villinger, H.W., Klaus, A., *Proc. ODP, Init. Repts.,* 205, 1–36 [CD-ROM]. Available from: Ocean Drilling Program, Texas A&M University, College Station TX 77845-9547, USA. [**HTML**]

Kastner, M., Morris, J., Chan, L.H., Saether, O., and Luckge, A., 2000. Three distinct fluid systems at the Costa Rica subduction zone: chemistry, hydrology, and fluxes. *Goldschmidt 2000, J. Conf. Abstr.,* 5:572. (Abstract)

Kimura, G., Silver, E.A., Blum, P., et al., 1997. *Proc. ODP, Init. Repts.,* 170: College Station, TX (Ocean Drilling Program). [**HTML**]

Langseth, M.G., and Silver, E.A., 1996. The Nicoya convergent margin: a region of exceptionally low heat flow. *Geophys. Res. Lett.,* 23:891–894.

Morris, J.D., Villinger, H.W., Klaus, A., et al., 2003. *Proc. ODP, Init. Repts.,* 205 [CD-ROM]. Available from: Ocean Drilling Program, Texas A&M University, College Station TX 77845-9547, USA. [**HTML**]

Paytan, A., Kastner, M., Martin, E., Macdougall, J., and Herbert T., 1993. Marine barite as a monitor of seawater strontium isotope composition. *Nature (London, U. K.),* 366:445–449. **doi:10.1038/366445a0**

Rubey, W.W., 1951. Geologic history of sea water: an attempt to state the problem. *Geol. Soc. Amer. Bull.,* 85:1485–1492.

Schilling, J.-G., Unni, C.K., and Bender, M.L., 1978. Origin of chlorine and bromine in the oceans. *Nature (London, U. K.),* 273:631–636. **doi:10.1038/273631a0**

Silver, E., Fisher, A., Saffer, D., Kastner, M., Morris, J., and McIntosh, K., 2000. Fluid flow paths in the Middle America Trench and Costa Rica margin. *Geology,* 28(8):679–682. **doi:10.1130/0091-7613(2000)028<0679:FFPITM>2.3.CO;2**

You C.-F., and Chan L.-H., 1996. Precise determination of lithium isotopic composition in low concentration natural samples. *Geochim. Cosmochim. Acta,* 60(5):909–915. **doi:10.1016/0016-7037(96)00003-8**

Figure F1. Depth profiles of F concentrations and F/Cl ratios in pore fluids from Sites (**A**, **D**) 1039/1253, (**B**, **E**) 1043/1255, and (**C**, **F**) 1040/1254. Saether's F concentration data from Sites 1039 and 1040 are also shown. SW = seawater.

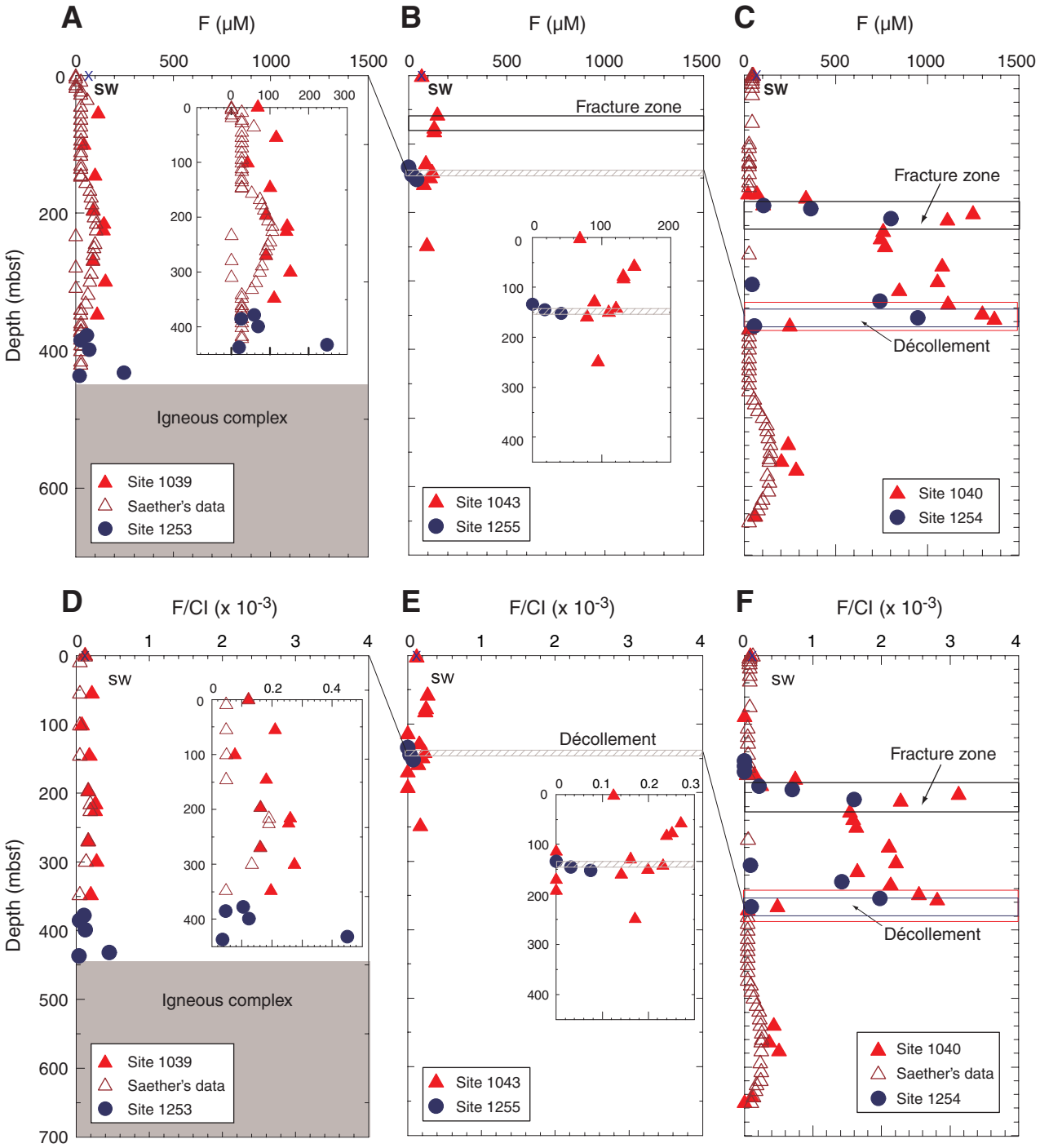

Figure F2. Depth profiles of Br concentrations and Br/Cl ratios in pore fluids from Sites (**A**, **D**) 1039/1253, (**B**, **E**) 1043/1255, and (**C**, **F**) 1040/1254. SW = seawater.

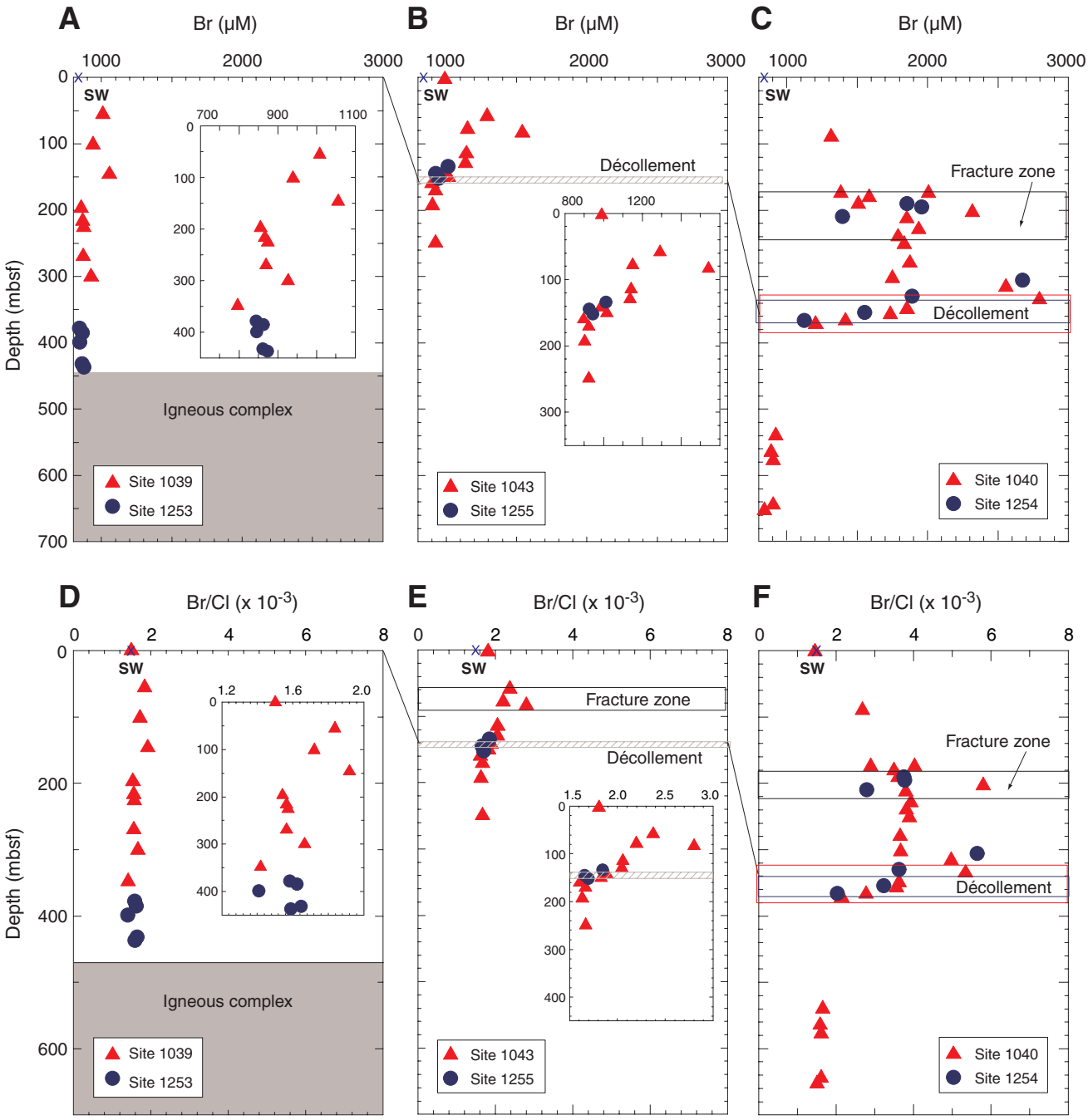

Figure F3. Relationships between F and Ca concentrations in pore fluids from Sites (A) 1039/1253, (B) 1043/1255, and (C) 1040/1254. The décollement and fracture zone pore fluids at Sites 1040/1254 have the highest F and Ca concentrations. Ca data for Sites 1253, 1254, 1255 are from Morris, Villinger, Klaus, et al. (2003), and data for Sites 1039, 1040, 1043 are from Kimura, Silver, Blum, et al. (1997). SW = seawater.

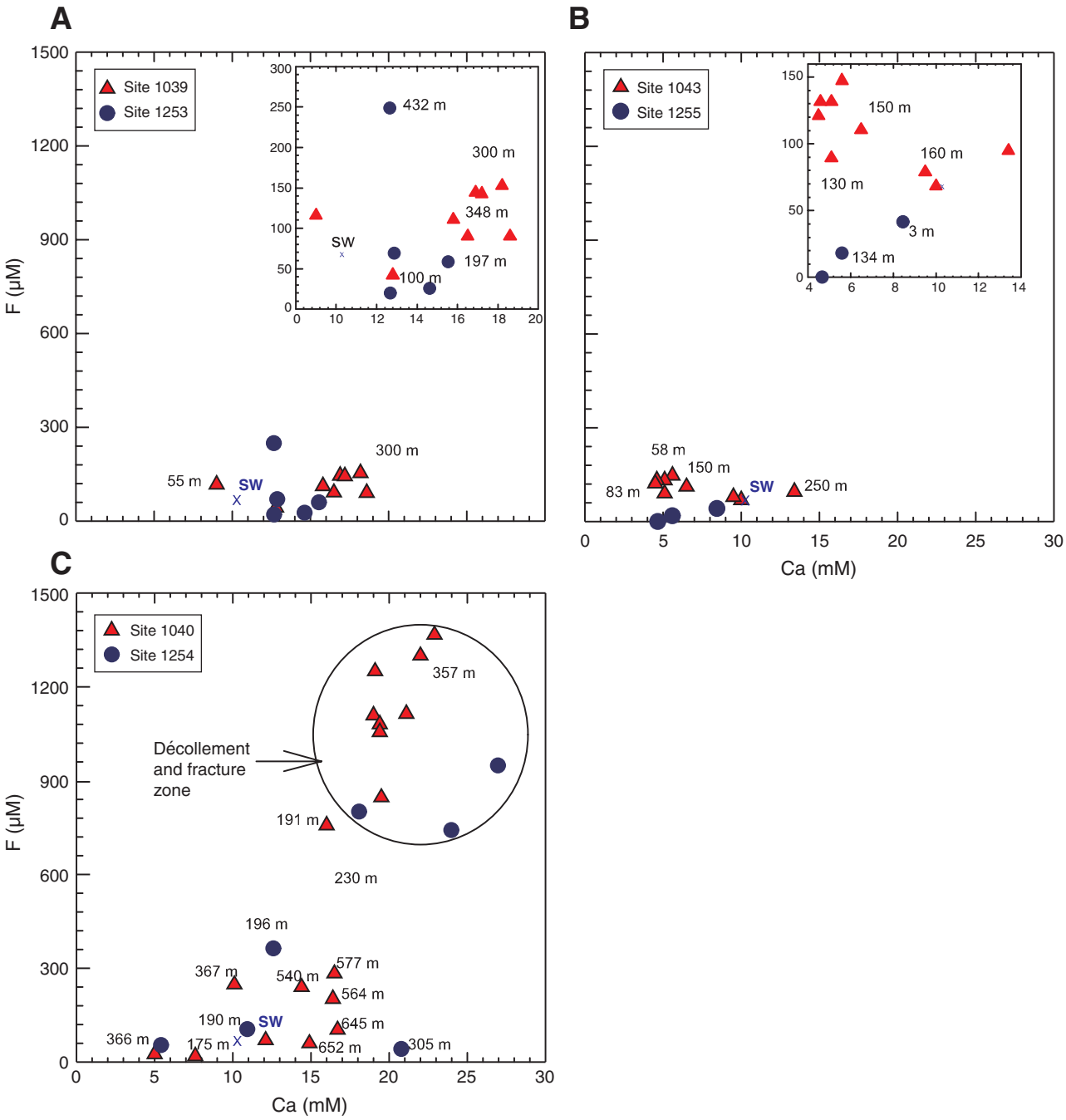

Figure F4. Depth profiles of (A) Rb and (B) Cs concentrations in pore fluids at Sites 1039 and 1253. Shaded areas designate a sill and the igneous complex. SW = seawater.

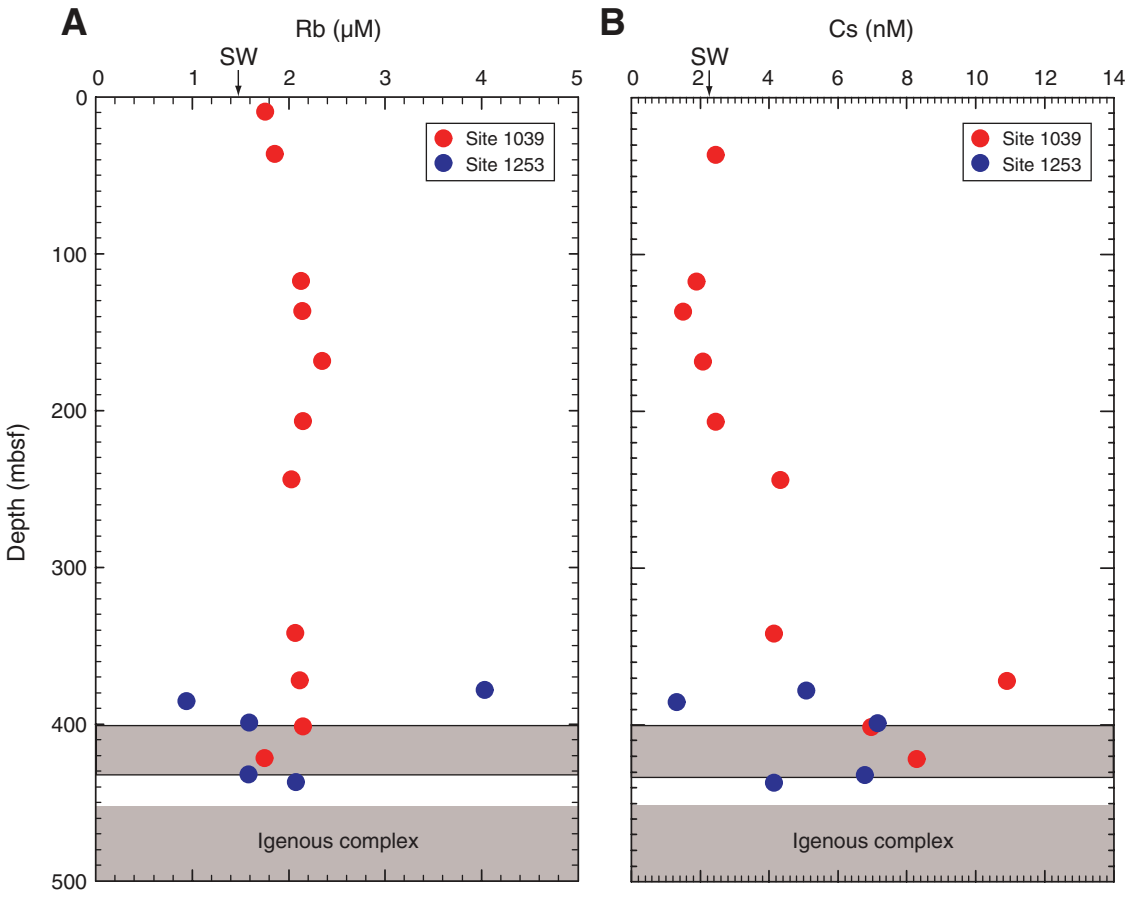

Figure F5. Depth profiles of (**A**) K and (**B**) Rb concentrations in pore fluids at Sites 1040 and 1254. K data for Site 1039 are from Kimura, Silver, Blum, et al. (1997), and data for Site 1253 are from Morris, Villinger, Klaus, et al. (2003). SW = seawater.

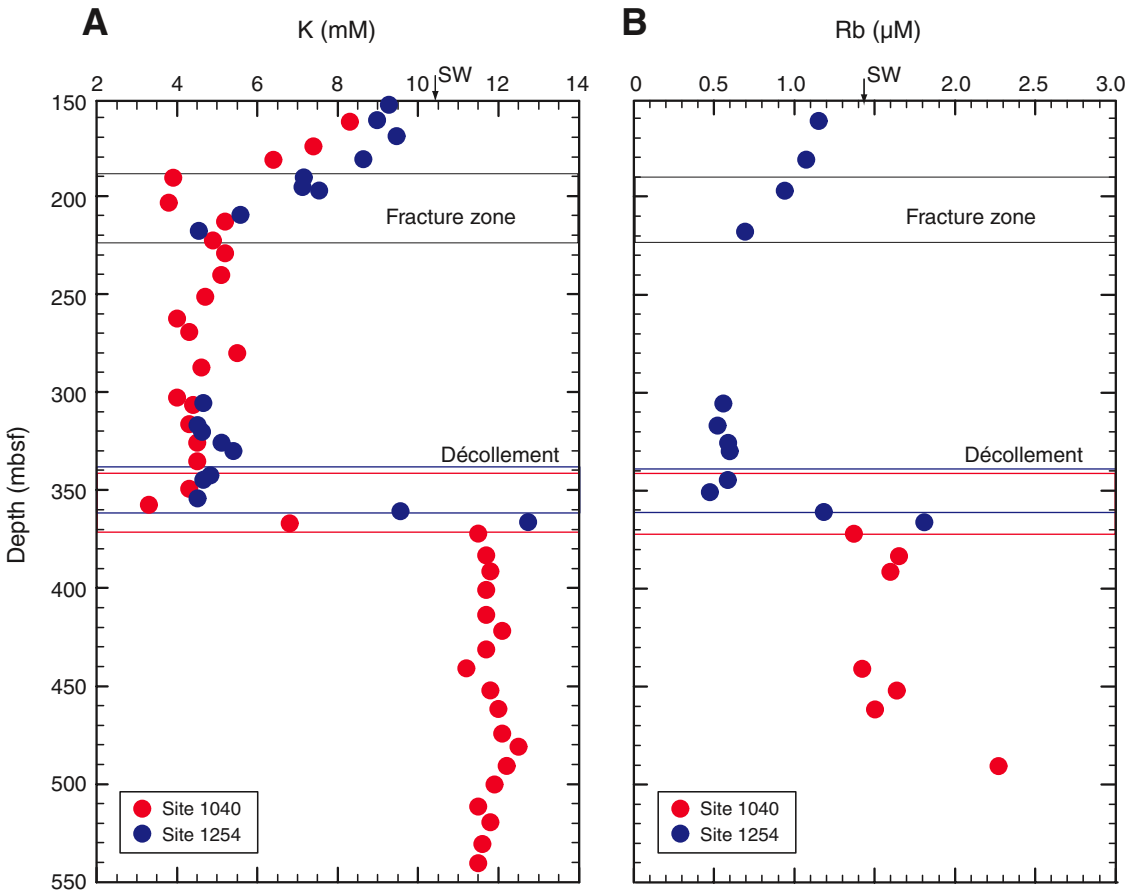

Figure F6. Depth profiles of (**A**) Rb, (**B**) Cs, and (**C**) Ba concentrations in bulk sediments at Sites 1039 and 1253. Ba concentration data are from Solomon et al. (this volume). ICP-MS = inductively coupled plasma–mass spectroscopy, XRF = X-ray fluorescence.

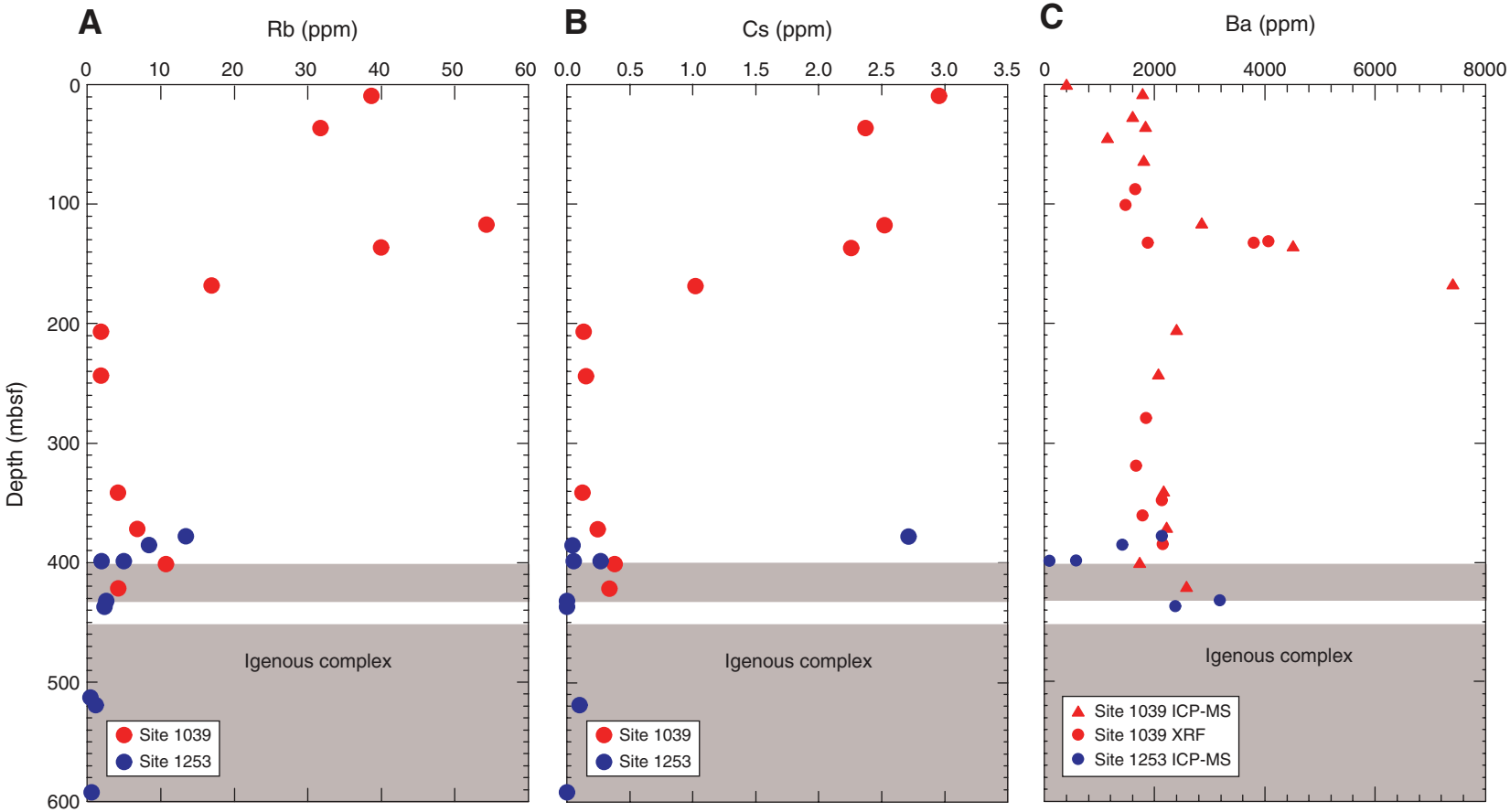

Figure F7. Depth profiles of (**A**) Rb, (**B**) Cs, and (**C**) Ba concentrations in bulk sediments at Sites 1040 and 1254. Ba concentration data are from **Solomon et al.** (this volume). ICP-MS = inductively coupled plasma–mass spectroscopy, XRF = X-ray fluorescence.

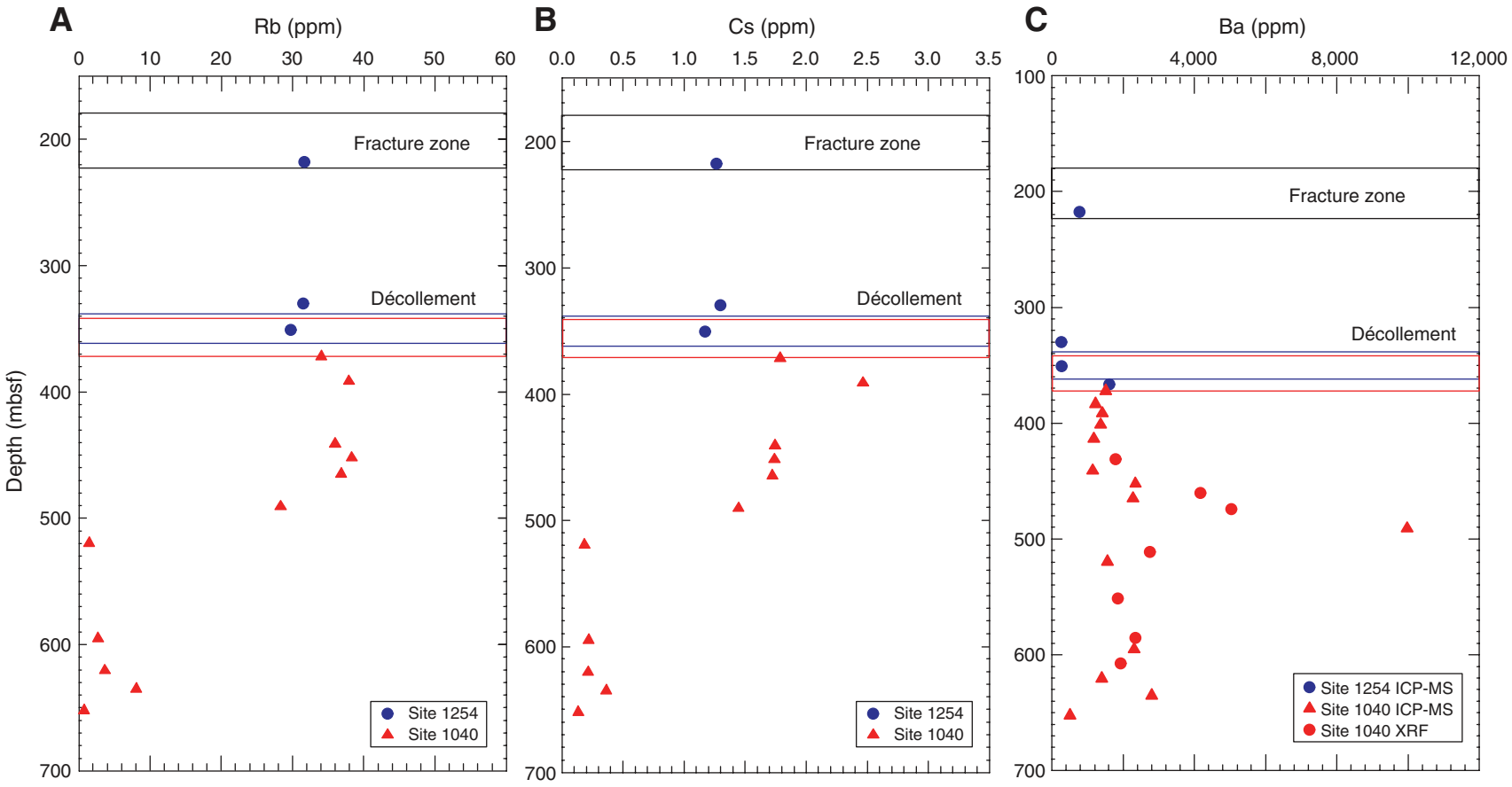

Figure F8. Depth profiles of Ba concentrations in pore fluids at Sites (**A**) 1039/1253 and (**B**) 1040/1254. Data are from **Solomon et al.** (this volume). BW = bottom water. ICP-OES = inductively coupled plasma–optical emission spectrometer, ICP-MS = inductively coupled plasma–mass spectroscopy.

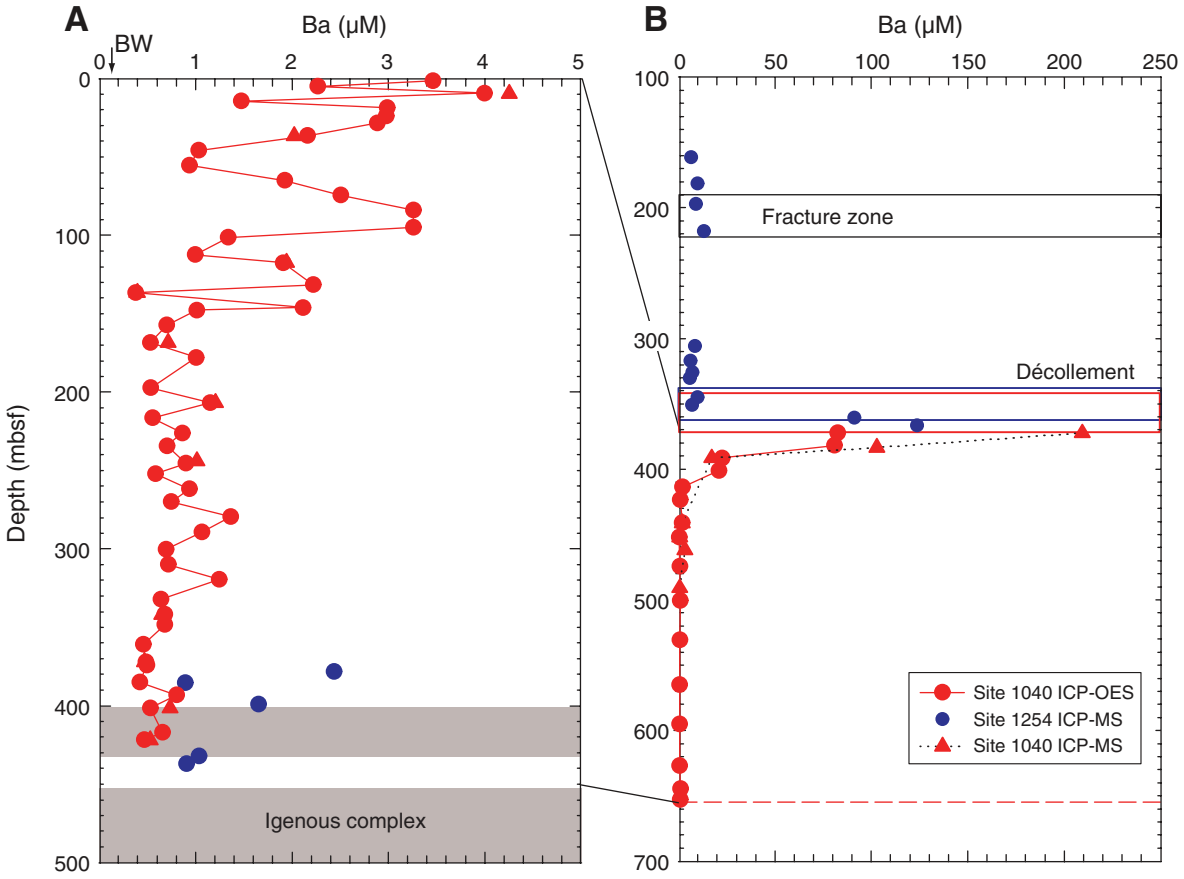

Figure F9. Mixing relationships between $^{87}Sr/^{86}Sr$ ratios and 1/Sr concentrations in pore fluids from Sites (A) 1039/1253, (B) 1043/1255, and (C) 1040/1254. The décollement and fracture zones are circled. Sr concentration data for Sites 1253–1255 are from Morris, Villinger, Klaus, et al. (2003). SW = seawater.

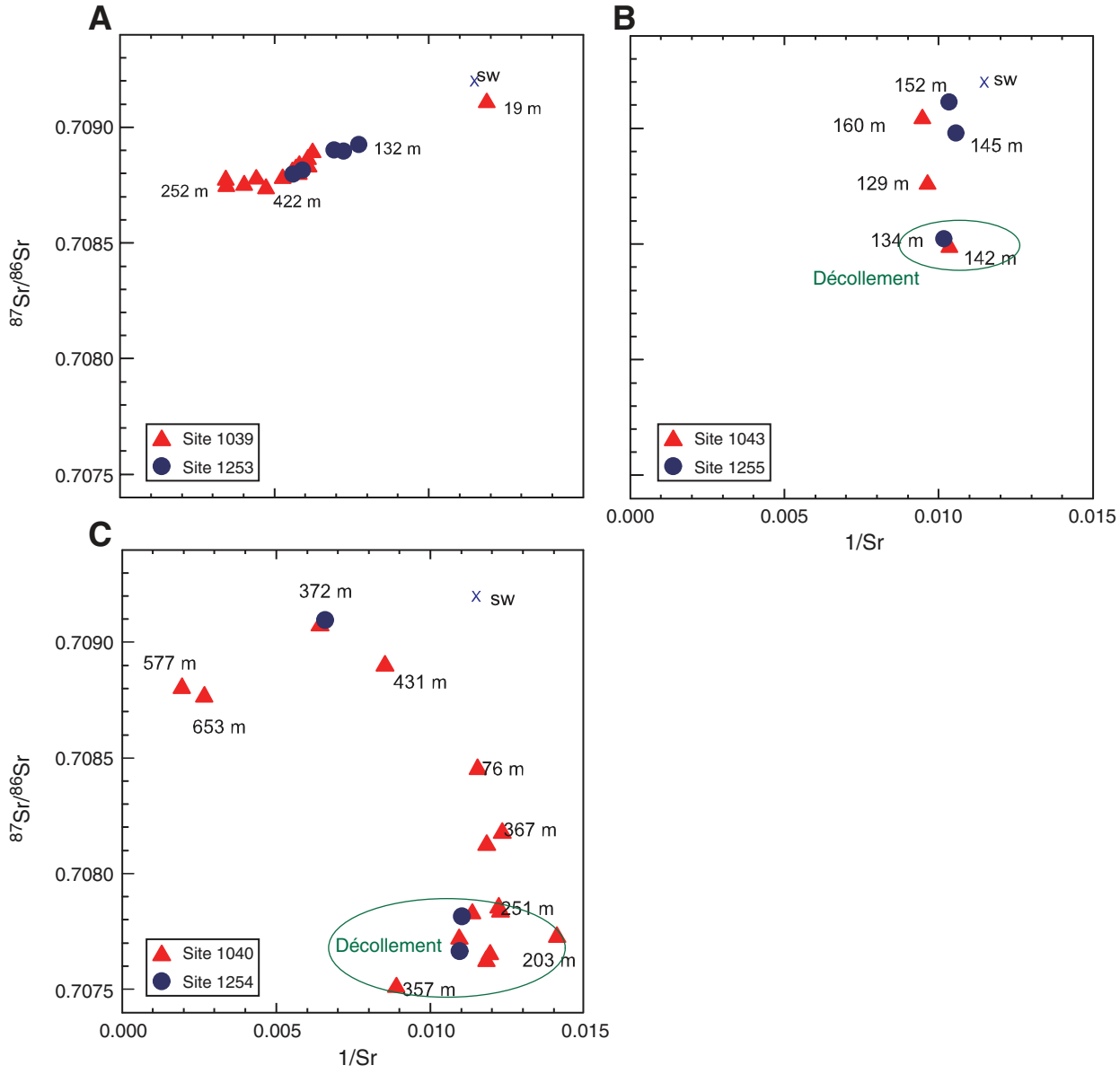

Figure F10. Depth profiles of δ^7Li in pore fluids from Sites (**A**) 1039 and (**B**) 1040/1254. Data for Sites 1039 and 1040 are from Chan and Kastner (2000). SW = seawater.

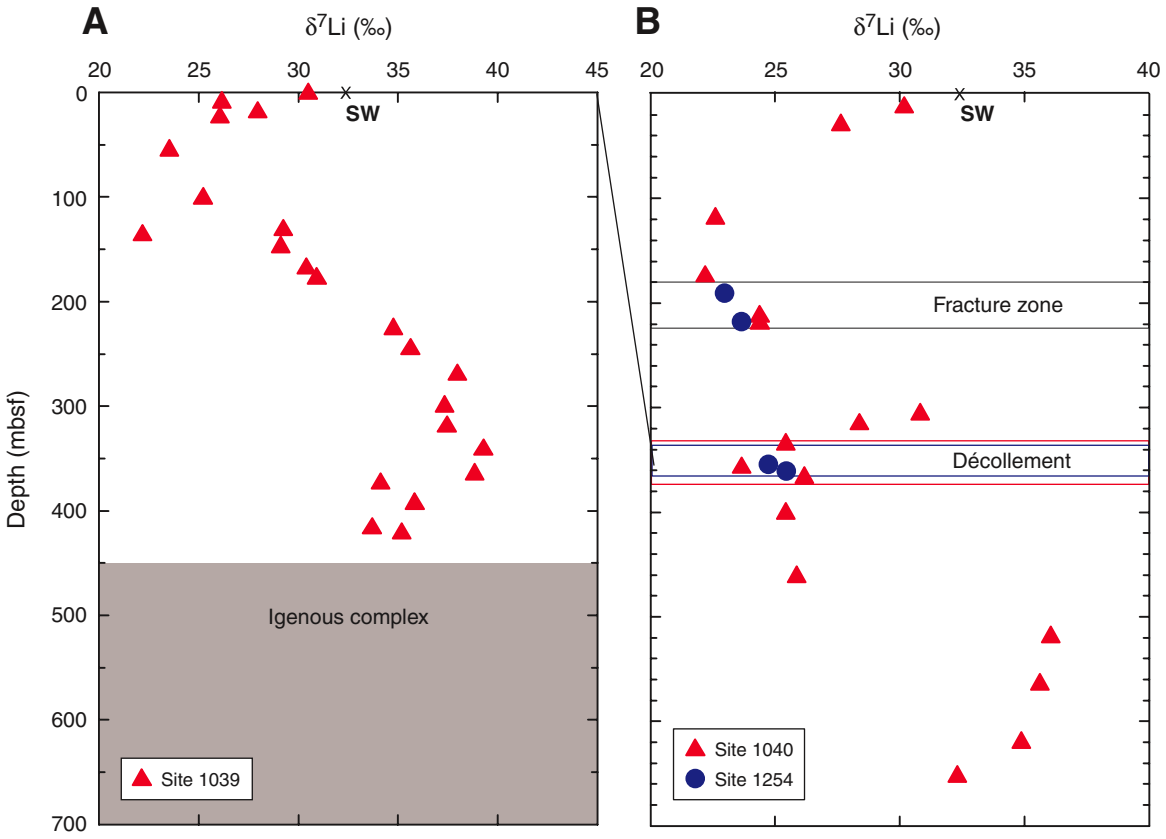

Figure F11. Depth profiles of $^{87}Sr/^{86}Sr$ ratios in pore fluids from Sites (**A**) 1039/1253, (**B**) 1043/1255, and (**C**) 1040/1254. SW = seawater.

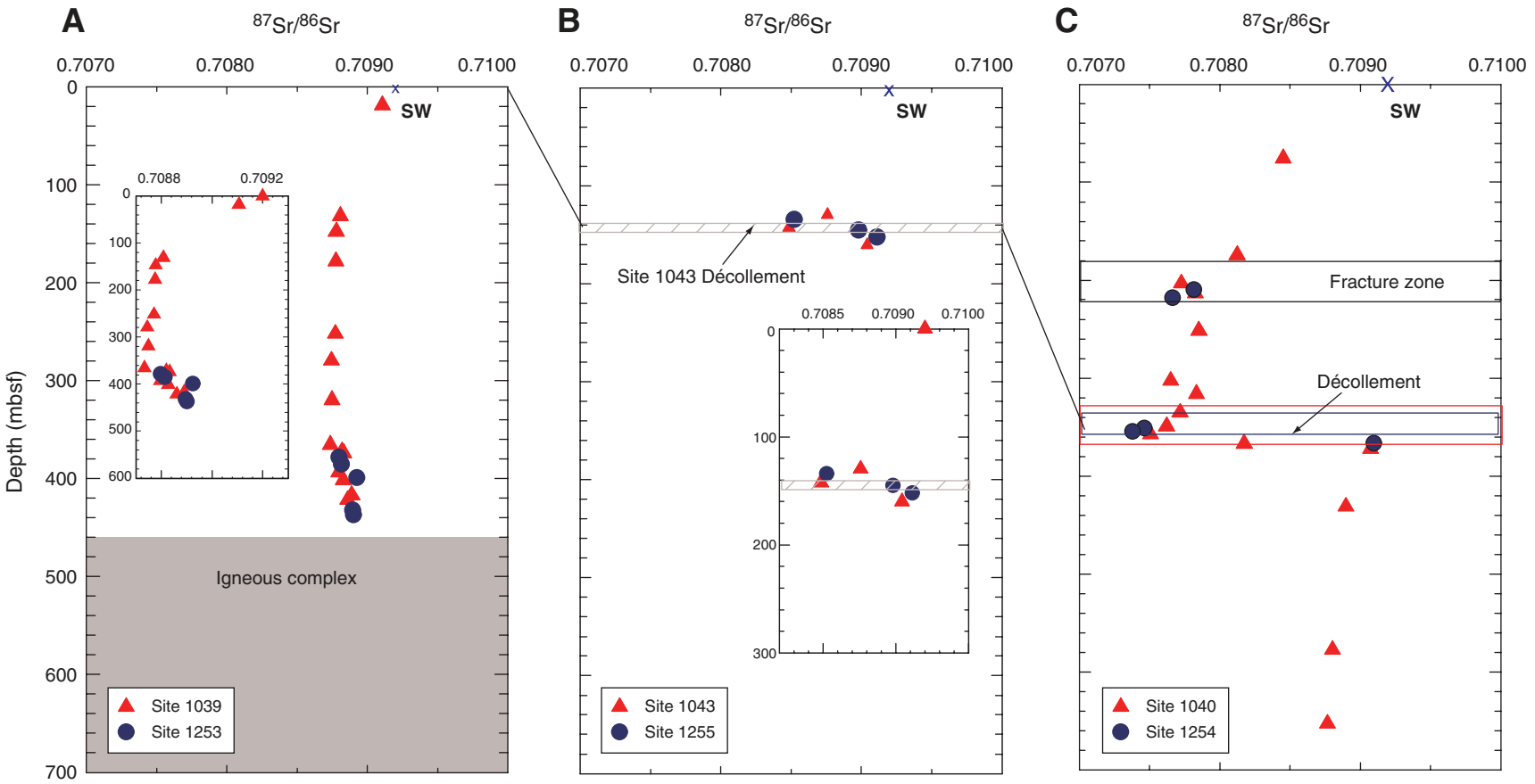

Table T1. Pore fluid chemical and Sr and Li isotopic compositions.

Core, section, interval (cm)	Depth (mbsf)	Salinity	Cations and anions (mM)						Trace elements (μM)								Isotopes (‰)	
			Cl	SO_4	Na	Mg	K	Ca	Ba*	Rb*	Cs*	Li	Sr	F*	Br*	$^{87}Sr/^{86}Sr$*	δ^6Li*	δ^7Li*
205-1253A-																		
1R-1, 13–29	370.2	35.0	559	28.00	480.81	46.20	12.00	15.73	2.27			10.50	189.83					
2R-2, 85–104	378.1	35.0	560	27.21	479.27	46.78	12.15	15.54	1.60			11.27	178.60	59	844	0.7087979		
3R-1, 7–23	385.4	35.0	560	28.56	485.07	46.35	11.79	14.63	1.04			13.51	169.40	25	863	0.7088139		
4R-3, 100–120	399.0	34.3	551	28.09	482.18	46.22	8.63	12.87	4.84			18.00	129.39	69	846	0.7089248		
10R-2, 59–73	432.1	35.5	563	27.81	495.82	44.41	10.45	12.65	3.02			17.50	138.23	248	862	0.7088959		
11R-1, 81–96	437.0	35.0	559	28.16	486.89	47.05	10.72	12.68	1.29			16.95	144.30	20	874	0.7089015		
205-1255A-																		
2R-2, 0–43	134.2	32.0	549	0.00	452.34	38.08	11.18	4.66	9.29			32.89	98.42	0	1012	0.7085221		
3R-2, 87–127	145.0	33.0	559	7.25	479.42	46.05	13.42	5.60	4.04			30.91	94.76	18	926	0.7089790		
4R-1, 0–38	152.2	34.0	557	8.61	472.81	45.09	12.74	8.45	3.15			26.69	96.74	42	945	0.7091124		
205-1254A-																		
1R-3, 52–87	153.7	28.0	496	0.00	426.79	22.62	9.28	7.34	ND	ND	ND	51.33	79.50					
2R-4, 125–160	161.4	29.0	513	1.08	446.76	24.02	8.98	5.69	6.67	1.15	5.27	51.84	83.38					
3R-3, 125–165	169.6	28.0	519	0.00	449.68	23.39	9.46	6.54	10.76	ND	ND	53.06	84.08					
4R-5, 45–90	181.3	28.0	507	0.00	434.71	23.37	8.63	8.46	9.74	1.08	3.57	50.78	85.26					
5R-5, 50–90	190.6	28.0	494	0.00	420.34	22.34	7.16	10.91	8.55	ND	ND	57.36	82.7	105	1855		–22.45	22.97
6R-1, 121–162	195.5	27.0	519	0.00	441.31	22.70	7.12	12.58	11.54	ND	ND	71.88	86.93	363	1959			
6R-2, 125-166	197.2	28.0	516	0.00	435.91	22.63	7.53	13.65	9.02	0.94	4.51	66.94	88.43					
7R-5, 34–74	209.8	29.0		0.00	ND	19.69	5.58	18.06	10.77	ND	ND	135.69	90.77	801	1395	0.7078145		
8R-4, 0–45	217.9	25.0	406	0.00	328.54	17.68	4.54	18.78	13.21	0.69	6.77	229.14	91.40			0.7076646	–23.10	23.65
9R-5, 0–40	305.7	26.0	474	0.00	389.76	19.03	4.65	20.77	8.37	0.56	9.59	125.10	77.11	42	2676			
10R-6, 0–40	316.9	27.0	469	0.00	384.05	19.26	4.51	20.96	6.37	0.52	4.70	129.99	84.82					
11R-1, 78–117	320.3	28.0	474	0.00	386.48	19.90	4.62	21.55	ND	ND	ND	133.82	97.28					
11R-5, 63–103	325.9	28.5	494	0.00	403.83	20.23	5.11	22.30	7.26	0.59	3.95	ND	ND					
12R-1, 101–141	330.1	31.0	522	0.00	427.39	20.64	5.40	23.97	5.69	0.60	4.14	121.67	95.20	742	1890			
13R-3, 100–145	342.7	25.5	484	0.00	399.28	17.31	4.83	22.64	ND	ND	ND	ND	ND					
13R-5, 69–109	344.9	25.0		0.00	ND	18.18	4.65	23.01	9.95	0.59	ND	171.47	90.95					
14R-3, 0–40	351.0		431	0.00	ND	ND	ND	ND	7.01	0.48	ND	ND	ND			0.7074641		
14R-6, 52–97	354.5	27.0	480	0.00	389.15	16.22	4.51	26.95	11.17	ND	ND	239.18	112.76	948	1553	0.7073788	–24.13	24.73
15R-3, 0–44	360.9	32.0	556	1.92	460.97	29.92	9.56	14.73	91.10	1.18	ND	69.69	168.18				–24.81	25.44
16R-3, 49–89	366.4	32.0	553	0.00	444.16	42.66	12.74	5.39	123.57	1.81	1.32	25.96	152.00	54.7	1124	0.7090958		

Notes: * = analyzed at Scripps Institution of Oceanography. All other data are from Morris, Villinger, Klaus, et al. (2003). ND = no data.

Table T2. Sediment Ba, Rb, and Cs concentrations.

Core, section, interval (cm)	Depth (mbsf)	Lithology	Ba (ppm)	Rb (ppm)	Cs (ppm)
170-1039B-					
1H-1, 145–150	1.45	Diatomaceous ooze with interbedded silt, sand	400.0	ND	ND
2H-5, 140–150	9.45	Diatomaceous ooze with radiolarians	1786	38.68	2.95
4H-5, 140–150	28.45	Siliceous ooze with minor ash	1598	ND	ND
5H-4, 140–150	36.45	Silty siliceous and diatomaceous ooze	1834	31.76	2.37
6H-4, 140–150	45.93	Siliceous ooze with minor ash	1148	ND	ND
8H-4, 140–150	64.95	Siliceous ooze with minor ash	1804	ND	ND
14X-3, 135–150	117.53	Silty clay with radiolarians and diatoms	2852	54.33	2.52
16X-3, 135–150	136.55	Clay with calcareous layers and ash	4512	39.98	2.26
19X-5, 135–150	168.45	Clayey biogenic ooze	7408	16.93	1.02
23X-5,135–150	206.85	Nannofossil ooze with diatoms	2394	1.851	0.135
27X-4, 135–150	243.85	Siliceous nannofossil ooze	2067	1.856	0.153
37X-5, 130–150	341.70	Siliceous nannofossil ooze	2165	4.19	0.123
40X-6, 130–150	372.00	Matrix supported breccia, biogenic ooze	2216	6.825	0.243
170-1039C-					
5R-1, 0–6	401.50	Nannofossil ooze with diatoms	1724	10.72	0.381
7R-1, 85–100	421.65	Diatomaceous nannofossil ooze	2580	4.208	0.347
205-1253A-					
2R-2, 85–104	378.10	Clay with nannofossils and ash	2134	13.44	2.71
3R-1, 7–23	385.40	Nannofossil chalk with foraminifers + clay rich laminations	1413	8.404	0.044
4R-3, 91–93	398.80	Silicic ash with clay and opaques (“big white ash”	572.4	4.980	0.053
4R-3, 100–120	399.00	Nannofossil chalk with clay and volcanic ash	93.19	1.969	0.268
10R-2, 59–73	432.10	Volcanic ash, nannofossils, clay mixed sediment	3180	2.612	BDL
11R-1, 81–96	437.00	Claystone with zeolites and spicules	2372	2.322	BDL
25R-1, 0–3	513.02	“Baked sediment” claystone with recrystallized calcite	281.2	0.4317	ND
27R-1, 7.5–9.0	519.34	“Baked sediment” claystone with recrystallized calcite and quartz	154.1	1.143	0.102
42R-2, 96–100	592.38	Green clay and zeolite vein	1.979	0.6167	BDL
205-1254A-					
8R-4, 0–45	217.90	Claystone	771.4	31.68	1.27
12R-1, 101–141	330.10	Calcite-rich claystone	269.1	31.49	1.30
14R-3, 0–40	351.00	Claystone with silt, ash, and opaques	277.0	29.73	1.17
16R-3, 49–89	366.40	Claystone with ash and diatoms	1614	ND	ND
170-1040C-					
23R-1 115–150	372.15	Dark olive-green silty clay with diatoms	1509	34.04	1.79
24R-2, 120–150	383.45	Sandy siltstone with diatoms	1221	ND	ND
25R-1, 125–150	391.58	Olive-green diatomaceous ooze with ash	1417	37.90	2.47
26R-1, 125–150	401.18	Diatomaceous silty clay	1371	ND	ND
27R-3, 125–150	413.78	Siliceous mudstone with ash	1176	ND	ND
30R-2, 125–150	441.05	Olive-green silty claystone	1147	35.98	1.74
31R-3, 125–150	452.18	Light grayish green silty claystone with ash	2351	38.29	1.74
32R-6, 14–17	465.04	Calcareous claystone with diatoms and ash	2284	36.84	1.72
35R-3, 132–150	490.82	Claystone with vitric ash and diatoms	9971	28.33	1.45
38R-3, 130–150	519.70	Siliceous nannofossil chalk	1562	1.440	0.184
46R-2, 130–150	595.20	Green diatomaceous chalk	2309	2.711	0.218
48R-6, 130–150	620.50	Diatomite with calcareous nannofossils	1397	3.662	0.214
50R-3, 130–150	635.20	Diatomite with nannofossils and ash	2796	8.073	0.364
52R-2, 74–80	652.27	Olive-green chalk with accessory zircon	514.1	0.7434	0.133

Note: ND = no data, BDL = below detection limit.